



Direct observation of phonon Anderson localization in Si/Ge aperiodic superlatticesRenjiu Hu  and Zhiting Tian ^{*}*Sibley School of Mechanical and Aerospace Engineering, Cornell University, Ithaca, New York 14853, USA*

(Received 6 June 2020; accepted 24 December 2020; published 15 January 2021)

Phonon Anderson localization has been receiving increasing interest in creating unique thermal transport properties. However, due to challenges to resolve and track the mode-specific transmission, the existence of phonon Anderson localization has only been inferred from the decay of overall thermal conductivity versus device length. In this work, we present direct evidence of phonon Anderson localization using the exponential decay of their mode-resolved transmissions. We clearly capture localized modes in different structures, even with a monotonically upward thermal conductivity trend.

DOI: [10.1103/PhysRevB.103.045304](https://doi.org/10.1103/PhysRevB.103.045304)**I. INTRODUCTION**

Anderson localization [1], a captivating phenomenon that was discovered more than half a century ago, never fails to fascinate researchers. It is now known that Anderson localization is a ubiquitous wave effect [2]. Besides being proposed in the electronic system, this phenomenon has been demonstrated in light [3,4], ultrasound [5,6], and ultracold atoms [7,8]. Thermal phonons, as quasiparticles, have both particle and wave natures. While the particle pictures have been extensively studied using the phonon Boltzmann transport equation, the wave picture is much less investigated. Phonon Anderson localization, originating from the wave interference, could potentially offer a new basis to minimize the thermal conductivity. For isotope-disordered nanotubes, the localization effects were not observable by a direct thermal conductivity measurement [9]. For aperiodic superlattices, the existence of phonon Anderson localization were inferred from the overall thermal conductivity behaviors. One criterion used to judge the existence of Anderson localization is the decreasing trend of the overall thermal conductivity as a function of device length [10–12]. A recent study [13] used machine learning to maximize Anderson localization for minimum thermal conductivity. These studies suggested the existence of phonon Anderson localization and inspired us to look deeper into the direct, mode-level proof of phonon Anderson localization.

In this work, we use the hallmark of Anderson localization to unambiguously demonstrate the existence of phonon Anderson localization at the mode level. To achieve this, we select materials with weak anharmonicity to minimize the decoherence from phonon-phonon interactions, leverage a recent development in the atomistic Green's function (AGF) method [14] to calculate the mode-specific transmission, and design a specific way to track the history of phonon transmission as we enlarge the device length. In Si/Ge aperiodic superlattices (ap-SLs), we observe the exponential decay of mode-resolved transmission vs SL length with an r -squared

value larger than 0.99. From the exponential decay, we are able to determine the mode-resolved localization lengths and show their spread at the same frequency. Moreover, we demonstrate that even when the thermal conductivity does not decrease with device length, vast localized modes could still exist. In other words, the macroscopic criterion based on overall thermal conductivity is a sufficient but not necessary condition for the existence of phonon Anderson localization.

Meanwhile, the mode-level analysis allows us to pin down three categories of modes—localized, propagating, and ballistic modes—and uncovers otherwise-buried information about different mode behaviors. We introduce the color-coded accumulative thermal conductivity curve to visualize the contributions from these three types of modes to thermal conductivity and their frequency distribution. We find that there is not a clean frequency cutoff between localized and delocalized modes and we could only define the onset frequency of the localization-dominant regime, which is related to the acoustic modes at the folded zone boundary. Our discovery offers insights into phonon Anderson localization and provides clear guidelines to identify the phonon localization. It can help the design of materials for technological areas where low thermal conductivity is required, including thermoelectrics, thermal insulation materials, and thermal barrier coatings, while guiding high-thermal-conductivity applications to avoid the localization.

II. METHOD

We apply AGF to calculate mode-resolved transmission. The traditional AGF [15–19] can only give frequency-dependent transmission. Because there can be multiple modes at a given frequency with distinct behaviors (as shown later), the frequency-dependent transmission cannot be used to identify mode localization. Thanks to the recent developments [14,20], we can now resolve the transmission at the mode level. We use Si/Ge periodic SL (p-SL) [Fig. 1(a)] as a benchmark for ap-SLs [Fig. 1(b)]. Unlike the previous studies, we particularly employ periodic Si/Ge SL as the leads, so that phonon modes entering the central region are all allowable

^{*}Corresponding author: zhiting@cornell.edu

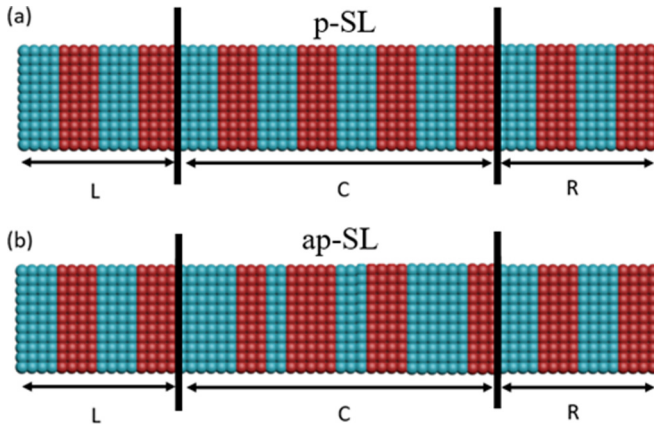


FIG. 1. Schematic of AGF setup. Left (L) and right (R) leads are comprised of Si/Ge p-SL and the central (C) region is the device of our interest. (a) p-SL and (b) ap-SL systems in the central region with one superperiod length. Blue and red refer to Si and Ge atoms, respectively.

modes in the p-SLs and the evanescent waves are minimized compared with using Si or Ge as the leads. The force constants for AGF inputs are obtained from first-principles calculations. The period length of p-SL is $2a$, where a is the lattice constant. Note that we intentionally select a small period length to have large enough disorder for ap-SL and the small distance between interfaces (smaller than the phonon coherence length) is critical to sustaining coherent interference. The details of the mode-specific AGF method could be found in Appendix A.

We introduce the concept of the superperiod to track the transmission of a given mode. For p-SL, eight periods are used to construct a superperiod of $16a$. For ap-SL, the length of each superperiod is $16a$ and the number of interfaces is kept at 15 within every superperiod, and within every superperiod the interfaces are randomly placed. We keep the same interface density for p-SL and ap-SL to have a fair comparison between them. To enlarge the central region, we attach new superperiods to the existing central region. We use the superperiod instead of completely randomly placed interfaces in the whole central region to make sure that we track modes with the same historical path as the length enlarges. We study two types of ap-SLs: mild and wild. If we set the constraint of only allowing the random displacement of interfaces within one atomic layer away from the corresponding p-SL interfaces, it is regarded as mild ap-SL; if the positions of interfaces are completely random within each superperiod, it is called wild ap-SL. The randomness of mild ap-SL and wild ap-SL structures are totally different (see the Supplemental Material [21]). We use $1a \times 1a$ in the transverse direction with 10×10 transverse k points after the convergence check (see the Supplemental Material [21]). As we use perfect interfaces, larger lateral size is not needed because the denser transverse k points can be translated to a larger cross section in the real space [14].

To classify the mode-level information, we define the following criteria to distinguish different types of modes via their transmission behaviors. If the transmission values of a mode at all the lengths are larger than 0.95, it is identified as a ballistic

mode. To find the localized modes, we use an exponential function to fit the transmission value versus the length of the central region. We set the threshold of the r -squared value at 0.99 for the fitting to be on the very conservative side and the majority of exponential decay modes have the r -squared value of 0.99 or larger (see the Supplemental Material [21]). Considering that not every mode starts the exponential decay from the first superperiod (see Appendix B), we search the decay start position from the first ($L = 8.75$ nm) to the tenth superperiod ($L = 87.5$ nm). We use at least three data points to make the fitting robust. The remaining modes, whose transmission values cannot be fitted by an exponential curve, are regarded as propagating modes. Both propagating and ballistic modes are heat conducting modes.

III. RESULTS

We first test mode decomposition on Si/Ge p-SL. The mode transmission in p-SL keeps at 1 with increasing length (Fig. S3 of the Supplemental Material [21]), which clearly shows ballistic transport in the p-SL case because the interference from coherent phonons forms a new dispersion for p-SL as if it is a homogenous material with the unit cell of a period [22]. Then we turn to the ap-SL case. At the extremely low-frequency region (< 0.7 THz), we could observe the existence of ballistic modes [Figs. 2(a) and 2(d)], just as those in the p-SL case, but with slight fluctuations. These long-wavelength phonons do not sense much of the disorder. For propagating modes, the transmission of propagating modes shows irregular, oscillating features [Figs. 2(b) and 2(e)]. Their transmission differs from the p-SL because the elastic scattering at the random interfaces disturb the ballistic transport. But we do not think these modes undergo the Fabry-Perot oscillation (see the Supplemental Material [21]). Most strikingly, we observed the hallmark of Anderson localization—the exponential decay of transmission with respect to the central region length—in both mild and wild ap-SLs [Figs. 2(c) and 2(f)]. This is direct evidence of phonon Anderson localization.

For the overall thermal conductivity, we confirm that the thermal conductivity of p-SL increases linearly with increasing length [Fig. 3(a)] due to the ballistic phonon transport. We plot the semilog version to better show the behavior of ap-SL and the linear plot can be found in the Supplemental Material [21]. In both ap-SL systems, a tremendous reduction of thermal conductivity is observed at every length compared to the p-SL. If we apply the previous criterion [10–12]—a reduction of thermal conductivity as a function of SL length after a critical size—only the wild ap-SL satisfies it. The mild ap-SL exhibits a generally increasing trend in its thermal conductivity, but it indeed has many localized modes. In other words, the macroscopic criterion is not a necessary condition to find phonon localization. Note that although we restricted the layer positions for the randomness to take place in mild ap-SL, there is a high interface density (15 interfaces in $16a$) as mentioned earlier. Thus, the disorder can be strong enough to generate Anderson localization in the mild case. In addition, three configurations of both mild and wild ap-SLs show a similar trend regardless of the exact placement of Si/Ge interfaces. This phenomenon shows that phonon Anderson

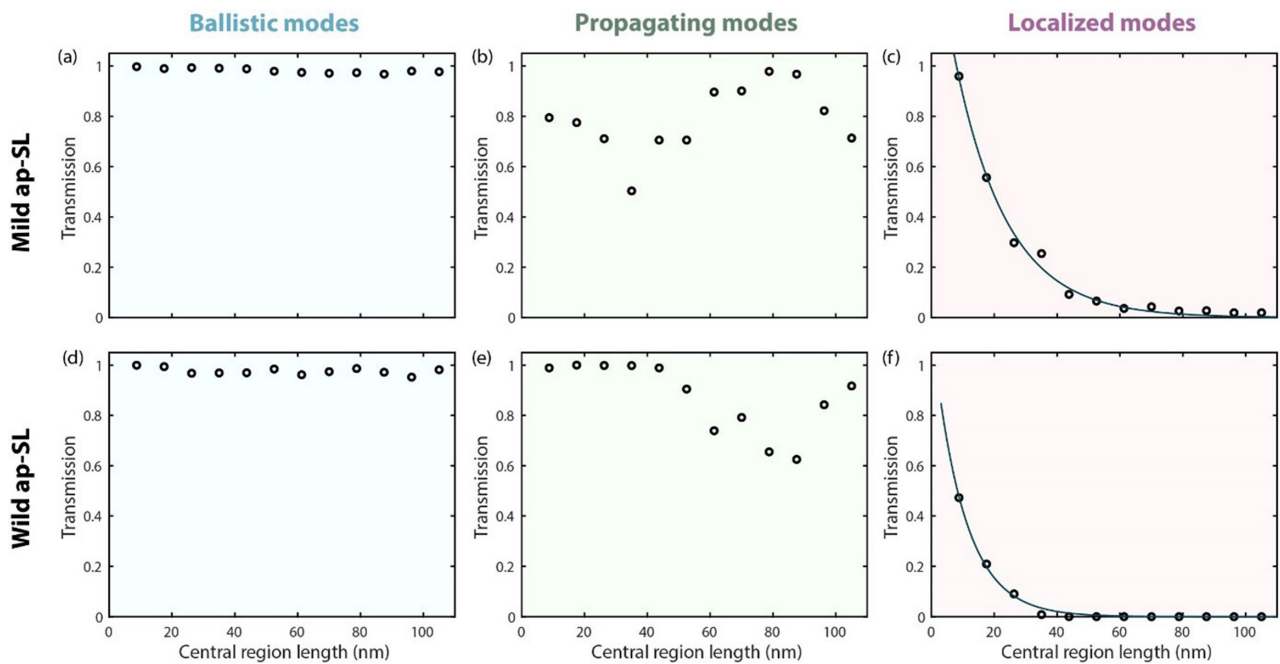


FIG. 2. The typical transmission pattern of (a) ballistic mode, (b) propagating mode, and (c) localized mode in mild ap-SL and (d) ballistic mode, (e) propagating mode, and (f) localized mode in wild ap-SL in the normal incident case.

localization is ubiquitous when the central region is sufficiently long and strongly disordered.

To gain a better insight, we separate the total thermal conductivity into three parts: contributions from ballistic,

propagating, and localized modes. In both mild and wild ap-SL cases, the thermal conductivity of localized modes has a similar decreasing trend with comparable values but the trends of conducting modes (ballistic and propagating modes) are

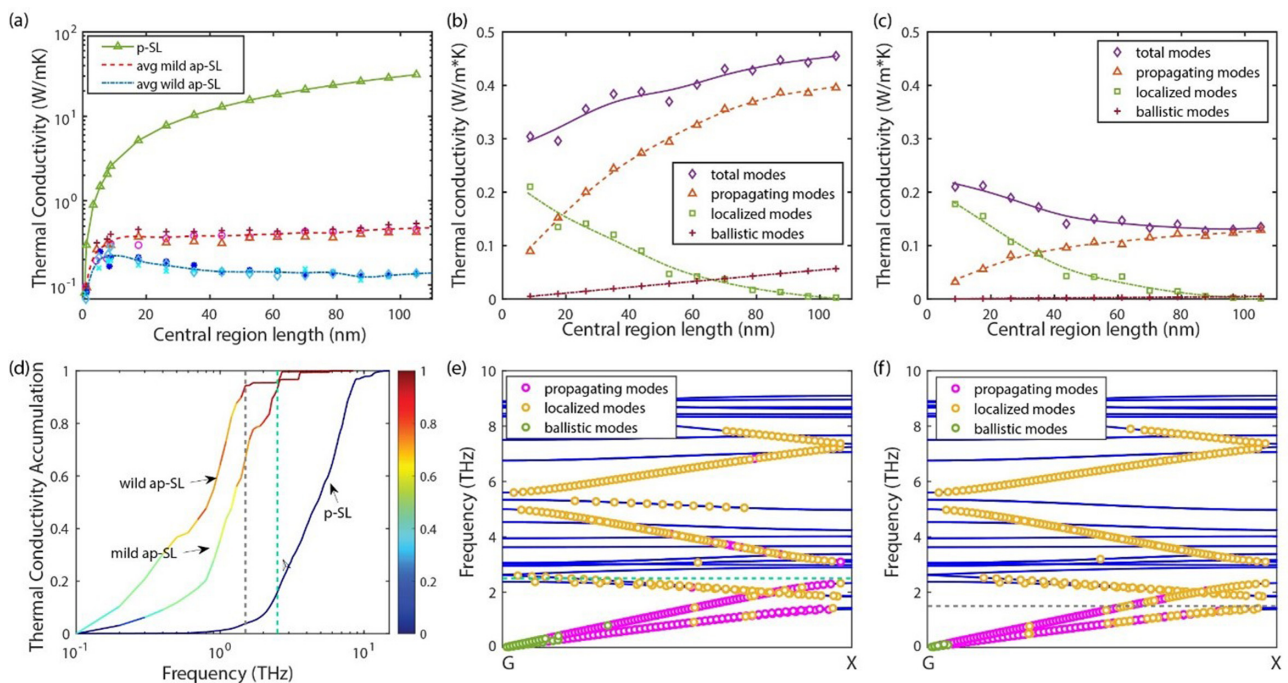


FIG. 3. (a) Thermal conductivities of Si/Ge p-SL and ap-SLs at 300 K. The red and blue dashed lines are the thermal conductivity of mild and wild ap-SLs averaged over three configurations, respectively. Panels (b) and (c) are the comparison of thermal conductivity contribution from all the modes, ballistic modes, propagating modes, and localized modes in mild ap-SL and wild ap-SL at 300 K, respectively. (d) Accumulative thermal conductivities vs frequency for p-SL and ap-SLs at 12th superperiod at 300 K. Phonon dispersion of p-SL along Gamma (G) to X with different types of modes at the normal incidence projected on it for (e) mild ap-SL and (f) wild ap-SL. Green and gray dash lines are the onset of the localization-dominant region of mild and wild ap-SL, respectively.

rather different [Figs. 3(b) and 3(c)]. In the mild ap-SL case, conducting modes have larger values and steeper increase than those in the wild ap-SL, which eventually overshadow the localized modes and make the overall trend of the total thermal conductivity upward. The mode-level contribution of different mode types to thermal conductivity is included in the Supplemental Material [21]. Notably, although the overall contribution of localized modes is masked from the total thermal conductivity trend in mild ap-SL, the mode-resolved transmission in this study allows us to capture those otherwise-buried localized modes.

To observe the mode distribution across the frequency range, we introduce color-coded thermal conductivity accumulation curves, as shown in Fig. 3(d). We use different colors to represent the averaged mode type at a given frequency among 100 k points. We digitize the ballistic modes with a given value of 0.01, propagating modes with a value of 0.5 and localized modes with a value of 0.99. Red suggests mostly localized modes at that frequency, blue suggests that ballistic modes dominate, and green marks propagating modes. While p-SL has a clean blue curve with all ballistic modes, ap-SLs show a gradual color change from cold to warm as the frequency increases. Due to different numbers of ballistic modes, we could barely see blue color in wild ap-SL but mild ap-SL has noticeable blue color in the lowest frequency range. We observe flat regions in the accumulative thermal conductivities in Fig. 3(d), indicating localized modes are dominant. The onsets of the localization-dominant regime are 2.5 and 1.5 THz for mild ap-SLs and wild ap-SLs, respectively.

To understand these different behaviors, we map the different modes onto the phonon dispersion of p-SL. Note that we use the dispersion of the bulk leads (periodic Si/Ge SL) rather than the central region to track the incident modes from the left lead. Due to the lack of periodicity, the phonon dispersion of ap-SLs cannot be defined. We discovered that in both ap-SLs, the vast majority of conducting modes concentrate on the acoustic branches and those onset frequencies for localization-dominant regimes approximately correspond to the frequency of LA branch and TA branch at the folded Brillouin zone boundaries, respectively [Figs. 3(e) and 3(f)]. It is interesting that only the lowest acoustic branches matter and even the higher-frequency-folded acoustic branches show very distinct mode characteristics. This is similar to a previous finding that the cutoff frequency of the totally coherent region of rough SLs is the lowest acoustic branch in the folded Brillouin zone [19]. The possible reasons are that phonons are easier to be localized near the band gap [11] and the lower frequency modes are less likely to be influenced by elastic interface scattering [10]. Comparing mild vs wild ap-SLs, the stronger disorder in wild ap-SL pushes the localization-dominant region to start at a lower frequency. While the previous works [23–25] showed the co-existence of different types of modes in a given system, a frequency cutoff was often defined between localized and delocalized modes. In other words, only one type of modes exists in a given frequency range in the traditional picture. However, Figs. 3(e) and 3(f) demonstrate that different types of modes co-exist either below or above the onset frequency. The mode-level

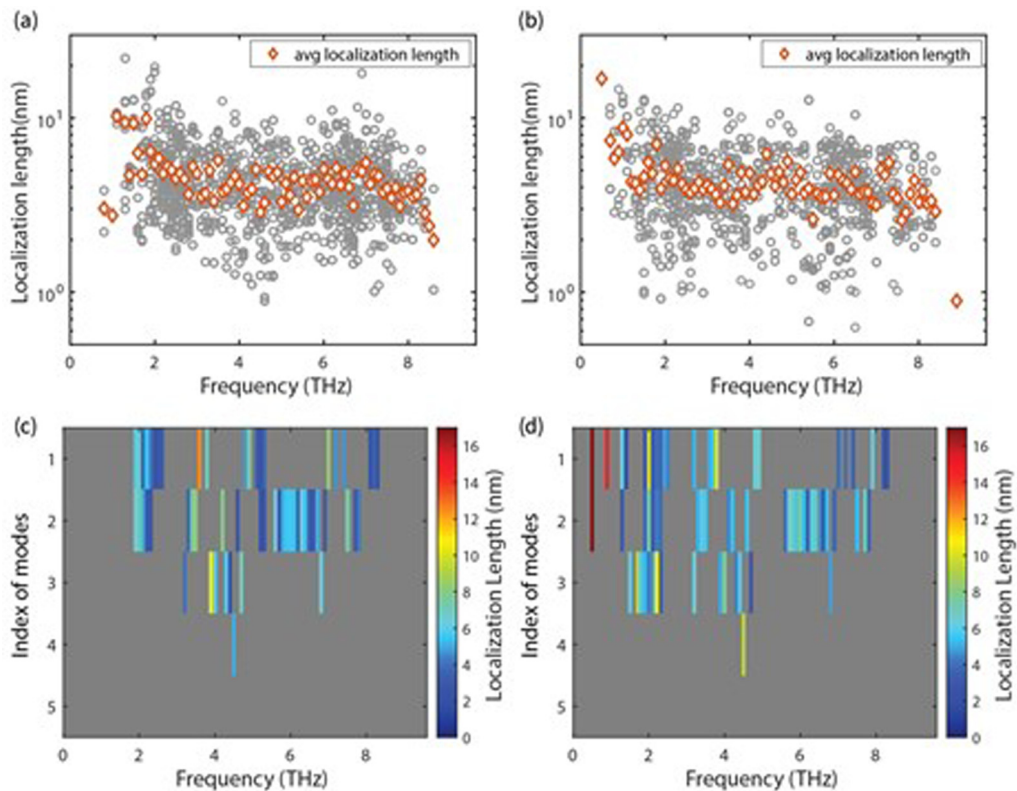


FIG. 4. Localization length of different modes (gray) and their frequency average (orange) in (a) mild and (b) wild ap-SL and the mode-level distribution of localization length in normal incident case of (c) mild and (d) wild ap-SL.

analysis reveals that there is not a clean cutoff frequency for different types of modes, although they tend to cluster in certain frequency ranges.

Localization length is the characteristic length that the transmission shrinks to $1/e$ of the initial transmission value. Note that previous studies used the fitting curve of the average frequency-dependent transmission of ap-SL to estimate the localization length [10,12]. Here the localization length is extracted directly from the exponential decay of the mode-specific transmission. We unveil that at a given frequency, the localization length has a spread among different modes [Figs. 4(a) and 4(b)]. Only the localized modes in the low-frequency range have longer localization lengths and the majority of the modes have localization lengths between 1 and 10 nm. The averaged localized lengths at a given frequency decrease quickly with increasing frequency and then flatten out. The trend is similar to the average localization length observed before [12] and these values are generally below the mean free path of Si or Ge at 300 K [26]. It further supports that anharmonic effects in Si/Ge SLs are negligible for Anderson localization at 300 K and below. It may seem counterintuitive that the largest average localization length of 16 nm exists in wild ap-SL instead of the mild one. But if we take a closer look at the normal incidence [Figs. 4(c) and 4(d)], wild ap-SL has its largest localization lengths in the low-frequency region (<0.7 THz), where mild ap-SL does not even have localized modes.

IV. CONCLUSION

We provide the direct observation of phonon Anderson localization at the mode level using the exponential decay of mode-resolved transmission. The Anderson localized modes could even be found when there is not a collective reduction of the overall thermal conductivity with respect to the device length. This finding reiterates the power of the mode-level analysis that enables us to uncover the hallmark of Anderson localization, with proper selection of the material system and careful design of transmission tracking. Meanwhile, the mode-level localization lengths are directly extracted from the exponential decay functions, which suggests that there is a span at a given frequency and in Si/Ge ap-SLs most of the localized modes have a localization length between 1 and 10 nm. There is no clean cutoff frequency for different types of modes and the onset frequency of localization-dominant region corresponds to acoustic modes at the folded zone boundary. Our proof of phonon Anderson localization as well as the knowledge enabled by the detailed mode analysis are helpful to advance our understanding of thermal transport in highly disordered materials and to enable controlling heat flow by leveraging or minimizing Anderson phonon localization for diverse thermal applications, ranging from thermoelectrics and thermal barrier coatings to thermal management.

ACKNOWLEDGMENTS

The authors acknowledge J. Dai for useful discussions. This work was sponsored by the Department of the Navy, Office of Naval Research under ONR Award No. N00014-18-

1-2724. This work used the Extreme Science and Engineering Discovery Environment (XSEDE), which is supported by National Science Foundation Grant No. ACI-1053575.

APPENDIX A: SIMULATION METHOD

Atomistic Green's function (AGF) is powerful to investigate interfacial thermal transport [15–17]. It has been extensively used on single Si/Ge interfaces to investigate phonon transport with the effect of strain [16], roughness [18], and lattice mismatch [27], but the application of that on Si/Ge superlattice is rare [19,22]. The (retarded) Green's function of the central region is

$$G(\omega) = [\omega^2 I - H_C - \Sigma_L(\omega) - \Sigma_R(\omega)]^{-1}. \quad (\text{A1})$$

Here, H_C is the dynamic matrix of the central region, which equals the harmonic force constants divided by mass, Σ_i ($i = L, R$) is the self-energy of both leads, which reflects the coupling between leads and central region, and I is the identity matrix that has the same size as H_C . We use QUANTUM ESPRESSO [28,29] along with PHONOPY [30] to calculate the force constants for the cubic unit cell of Si. The lattice constant for Si is $a = 0.357$ nm. For Ge atoms, we use the same lattice constant and force constants as Si but the mass of Ge. The frequency-dependent phonon transmission is given as

$$\Xi(\omega) = \text{Tr}[\Gamma_L(\omega)G(\omega)\Gamma_R(\omega)G^\dagger(\omega)], \quad (\text{A2})$$

where $\Gamma_i = i(\Sigma_i - \Sigma_i^\dagger)$ is the level-width function which indicates the leakage of phonons from leads and \dagger means the conjugated transpose. Using the Landauer formula, the thermal conductivity per unit area would be

$$\kappa = \frac{L}{S} \times \frac{1}{2\pi} \int_0^\infty \hbar\omega \frac{\partial f(\omega, T)}{\partial T} \Xi(\omega) d\omega. \quad (\text{A3})$$

Here, L and S are the length and cross-section area of the central region, respectively. f is the Bose-Einstein distribution.

To resolve the transmission at the mode level, we follow Ref. [14] and use the Bloch matrices, which could be presented as

$$F_L^{\text{adv}}(-)^{-1} = [H_L^{10} g_L^{\text{ret}}]^\dagger, \quad (\text{A4a})$$

$$F_R^{\text{ret}}(+) = g_R^{\text{ret}} H_R^{10}, \quad (\text{A4b})$$

where $g_{L,R}^{\text{ret}}$ is the retarded surface Green's function of left/right lead, $H_{L,R}^{10}$ is the dynamical matrix between two adjacent Si/Ge periods in the left or the right lead, and η is the infinitesimal value to represent phonon leakage from leads. The $+$ and $-$ signs denote the infinite extension to the right and left directions, respectively.

To gain the mode-specific information of the leads, we need mode decomposition:

$$F_L^{\text{adv}}(\pm) U_L^{\text{adv}}(\pm) = U_L^{\text{adv}}(\pm) \Lambda_L^{\text{adv}}(\pm), \quad (\text{A5a})$$

$$F_R^{\text{ret}}(\pm) U_R^{\text{ret}}(\pm) = U_R^{\text{ret}}(\pm) \Lambda_R^{\text{ret}}(\pm). \quad (\text{A5b})$$

Here, U_L^{adv} and U_R^{ret} are the normalized eigenstates in the left and right leads, respectively.

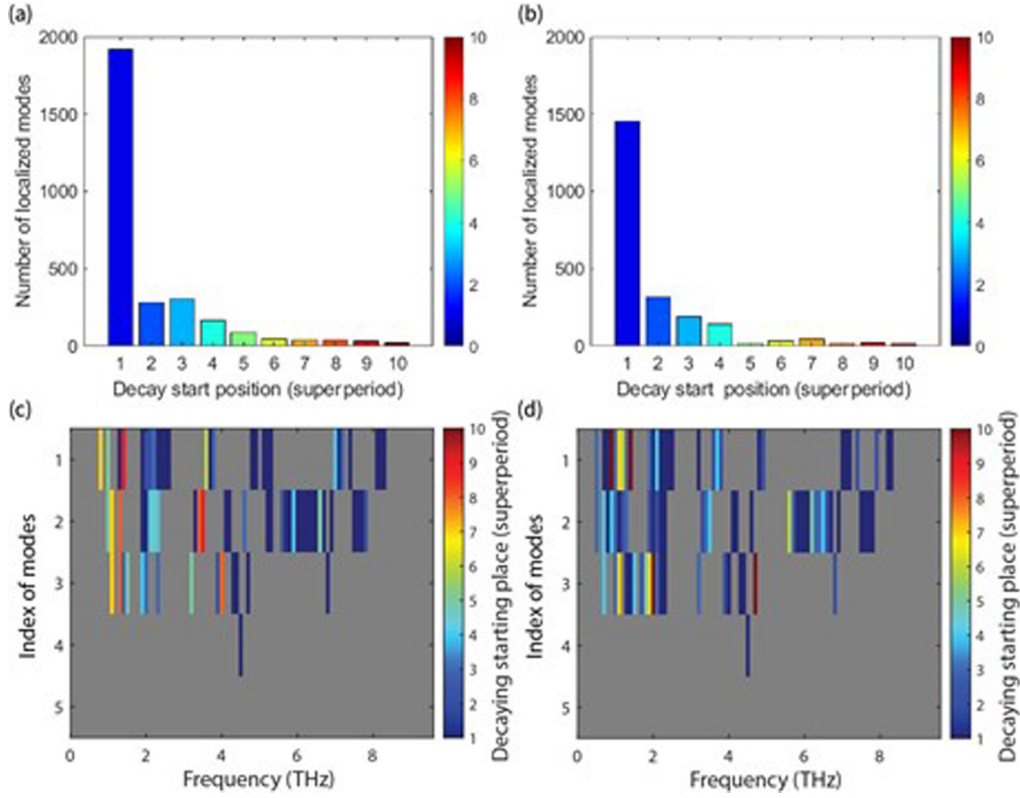


FIG. 5. The statistics of the localized modes and their decay start point in terms of superperiods in (a) mild ap-SL and (b) wild ap-SL and the mode-level information for normal incidence case in (c) mild ap-SL and (d) wild ap-SL.

Another necessary component is the velocity matrix of the leads,

$$V_L(-) = \frac{a_L}{2\omega} U_L^{\text{adv}}(-)^\dagger \Gamma_L U_L^{\text{adv}}(-), \quad (\text{A6a})$$

$$V_R(+) = \frac{a_R}{2\omega} U_R^{\text{ret}}(+)^{\dagger} \Gamma_R U_R^{\text{ret}}(+), \quad (\text{A6b})$$

where $a_{L,R}$ is the superperiod length of the left/right lead.

The transmission between individual phonon modes in the left lead and in the right lead is

$$t = \frac{2i\omega}{\sqrt{(a_L a_R)}} [V_R(+)]^{1/2} U_R^{\text{ret}}(+)^{\dagger} G_{RL}^{\text{ret}} [U_L^{\text{adv}}(-)^{\dagger}] [V_L(-)]^{1/2}. \quad (\text{A7})$$

All the mode-level transmission in this work is based on Eq. (A7).

We choose Si/Ge for the following reasons. Because the phonon-phonon scattering can lead to phase decoherence and destroy the Anderson localization, systems with weak anharmonicity is desired to probe the existence of localization. We meanwhile want to stay with the popular superlattice systems that have been mostly studied. Therefore, we compare Si/Ge and GaAs/AlAs SLs. The average Grüneisen parameters of Si, Ge, AlAs, and GaAs, at 300 K are 0.48, 0.75, 0.8, and 1.1, respectively [31,32]. The thermal conductivity of Si/Ge ap-SLs showed the Anderson localization behaviors at room temperature with anharmonicity included in MD simulations [12], which means the anharmonic effect is too weak to destroy the coherence at 300 K. GaAs/AlAs SLs doped with ErAs, on the other hand, showed thermal conductivity maximum

only below 100 K [10], which means that at room temperature the anharmonic effect leads to delocalization. Therefore, Si/Ge should have weaker anharmonicity than GaAs/AlAs. We should also note that the AGF is applied under the harmonic regime in this work. Despite our recent development on anharmonic AGF for 3D structures [33], it is still formidable to apply it to SLs with very long central regions and the mode decomposition has not been developed under the anharmonic AGF framework. But if we select a system with weak anharmonic effect that does not overshadow the phonon Anderson localization up to the room temperature, the harmonic calculation could in fact serve as a clean platform to observe the localization while largely representing the actual system.

APPENDIX B: DELOCALIZATION-LOCALIZATION TRANSITION

As mentioned in main text, not all the exponential decays start from the first superperiod and some modes might take longer to cultivate the localization behaviors. Therefore, we track the positions where the exponential decay starts as shown in Fig. 5. Most of the localized modes start their decay from the first superperiod but a few modes experience the delocalization-to-localization transition. At the mode level, low-frequency modes are more likely to start the decaying at a further place in general but at the same frequency, different modes start their decay at different places (Fig. 5). This reiterates the importance of resolving mode-level information that can be masked by frequency-dependent quantities.

- [1] P. W. Anderson, Absence of diffusion in certain random lattices, *Phys. Rev.* **109**, 1492 (1958).
- [2] P. Sheng and B. van Tiggelen, Introduction to wave scattering, localization and mesoscopic phenomena. second edition, *Waves Random Complex Media* **17**, 235 (2007).
- [3] D. S. Wiersma, P. Bartolini, A. Lagendijk, and R. Righini, Localization of light in a disordered medium, *Nature (London)* **390**, 671 (1997).
- [4] A. A. Chabanov, M. Stoytchev, and A. Z. Genack, Statistical signatures of photon localization, *Nature (London)* **404**, 850 (2000).
- [5] R. L. Weaver, Anderson localization of ultrasound, *Wave Motion* **12**, 129 (1990).
- [6] H. Hu, A. Strybulevych, J. H. Page, S. E. Skipetrov, and B. A. Van Tiggelen, Localization of ultrasound in a three-dimensional elastic network, *Nat. Phys.* **4**, 945 (2008).
- [7] J. Chabé, G. Lemarié, B. Grémaud, D. Delande, P. Szriftgiser, and J. C. Garreau, Experimental Observation of the Anderson Metal-Insulator Transition with Atomic Matter Waves, *Phys. Rev. Lett.* **101**, 255702 (2008).
- [8] J. Billy, V. Josse, Z. Zuo, A. Bernard, B. Hambrecht, P. Lugan, D. Clément, L. Sanchez-Palencia, P. Bouyer, and A. Aspect, Direct observation of Anderson localization of matter waves in a controlled disorder, *Nature (London)* **453**, 891 (2008).
- [9] I. Savić, N. Mingo, and D. A. Stewart, Phonon Transport in Isotope-Disordered Carbon and Boron-Nitride Nanotubes: Is Localization Observable?, *Phys. Rev. Lett.* **101**, 165502 (2008).
- [10] J. Mendoza and G. Chen, Anderson localization of thermal phonons leads to a thermal conductivity maximum, *Nano Lett.* **16**, 7616 (2016).
- [11] M. N. Luckyanova, J. Mendoza, H. Lu, B. Song, S. Huang, J. Zhou, M. Li, Y. Dong, H. Zhou, J. Garlow, L. Wu, B. J. Kirby, A. J. Grutter, A. A. Puretzky, Y. Zhu, M. S. Dresselhaus, A. Gossard, and G. Chen, Phonon localization in heat conduction, *Sci. Adv.* **4**, eaat9460 (2018).
- [12] T. Juntunen, O. Vänskä, and I. Tittonen, Anderson Localization Quenches Thermal Transport in Aperiodic Superlattices, *Phys. Rev. Lett.* **122**, 105901 (2019).
- [13] P. Roy Chowdhury, C. Reynolds, A. Garrett, T. Feng, S. P. Adiga, and X. Ruan, Machine learning maximized Anderson localization of phonons in aperiodic superlattices, *Nano Energy* **69**, 104428 (2020).
- [14] Z.-Y. Ong, Atomistic *S*-matrix method for numerical simulation of phonon reflection, transmission, and boundary scattering, *Phys. Rev. B* **98**, 195301 (2018).
- [15] N. Mingo and L. Yang, Phonon transport in nanowires coated with an amorphous material: An atomistic Green's function approach, *Phys. Rev. B* **68**, 245406 (2003).
- [16] W. Zhang, T. S. Fisher, and N. Mingo, Simulation of interfacial phonon transport in Si-Ge heterostructures using an atomistic Green's function method, *J. Heat Transfer* **129**, 483 (2007).
- [17] W. Zhang, N. Mingo, and T. S. Fisher, Simulation of phonon transport across a non-polar nanowire junction using an atomistic Green's function method, *Phys. Rev. B* **76**, 195429 (2007).
- [18] Z. Tian, K. Esfarjani, and G. Chen, Enhancing phonon transmission across a Si/Ge interface by atomic roughness: First-principles study with the Green's function method, *Phys. Rev. B* **86**, 235304 (2012).
- [19] Z. Tian, K. Esfarjani, and G. Chen, Green's function studies of phonon transport across Si/Ge superlattices, *Phys. Rev. B* **89**, 235307 (2014).
- [20] S. Sadasivam, U. V. Waghmare, and T. S. Fisher, Phonon-eigenspectrum-based formulation of the atomistic Green's function method, *Phys. Rev. B* **96**, 174302 (2017).
- [21] See Supplemental Material at <http://link.aps.org/supplemental/10.1103/PhysRevB.103.045304> for 1D chain model analysis, convergence check, and detailed mode level information.
- [22] M. N. Luckyanova, J. Garg, K. Esfarjani, A. Jandl, M. T. Bulsara, A. J. Schmidt, A. J. Minnich, S. Chen, M. S. Dresselhaus, Z. Ren, E. A. Fitzgerald, and G. Chen, Coherent phonon heat conduction in superlattices, *Science* **338**, 936 (2012).
- [23] J. L. Feldman, M. D. Kluge, P. B. Allen, and F. Wooten, Thermal conductivity and localization in glasses: Numerical study of a model of amorphous silicon, *Phys. Rev. B* **48**, 12589 (1993).
- [24] P. B. Allen, J. L. Feldman, J. Fabian, and F. Wooten, Diffusons, locons and propagons: Character of atomic vibrations in amorphous Si, *Philos. Mag. B* **79**, 1715 (1999).
- [25] W. Lv and A. Henry, Non-negligible contributions to thermal conductivity from localized modes in amorphous silicon dioxide, *Sci. Rep.* **6**, 35720 (2016).
- [26] D. Singh, J. Y. Murthy, and T. S. Fisher, Effect of phonon dispersion on thermal conduction across Si/Ge interfaces, *J. Heat Transfer* **133**, 122401 (2011).
- [27] X. Li and R. Yang, Effect of lattice mismatch on phonon transmission and interface thermal conductance across dissimilar material interfaces, *Phys. Rev. B* **86**, 054305 (2012).
- [28] P. Giannozzi, O. Andreussi, T. Brumme, O. Bunau, M. Buongiorno Nardelli, M. Calandra, R. Car, C. Cavazzoni, D. Ceresoli, M. Cococcioni, N. Colonna, I. Carnimeo, A. Dal Corso, S. de Gironcoli, P. Delugas, R. A. DiStasio, A. Ferretti, A. Floris, G. Fratesi, G. Fugallo *et al.*, Advanced capabilities for materials modelling with Quantum ESPRESSO, *J. Phys.: Condens. Matter* **29**, 465901 (2017).
- [29] P. Giannozzi, S. Baroni, N. Bonini, M. Calandra, R. Car, C. Cavazzoni, D. Ceresoli, G. L. Chiarotti, M. Cococcioni, I. Dabo, A. Dal Corso, S. de Gironcoli, S. Fabris, G. Fratesi, R. Gebauer, U. Gerstmann, C. Gougoussis, A. Kokalj, M. Lazzeri, L. Martin-Samos *et al.*, Quantum ESPRESSO: A modular and open-source software project for quantum simulations of materials, *J. Phys.: Condens. Matter* **21**, 395502 (2009).
- [30] A. Togo and I. Tanaka, First principles phonon calculations in materials science, *Scr. Mater.* **108**, 1 (2015).
- [31] T. Soma, Temperature dependence of the Grüneisen constant of Si and Ge, *Phys. Status Solidi* **82**, 319 (1977).
- [32] S. Adachi, Phonons and lattice vibronic properties, in *GaAs and Related Materials* (World Scientific, Singapore, 1994), pp. 70–111.
- [33] J. Dai and Z. Tian, Rigorous formalism of anharmonic atomistic Green's function for three-dimensional interfaces, *Phys. Rev. B* **101**, 041301(R) (2020).